
KAN-Koopman Based Rapid Detection Of Battery Thermal Anomalies With Diagnostics Guarantees

A PREPRINT

Sanchita Ghosh¹ and Tanushree Roy¹

¹Department of Mechanical Engineering, Texas Tech University, Lubbock, TX 79409, US.
Emails: sancghos@ttu.edu, tanushree.roy@ttu.edu.

February 25, 2026

ABSTRACT

Early diagnosis of battery thermal anomalies is crucial to ensure safe and reliable battery operation by preventing catastrophic thermal failures. Battery diagnostics primarily rely on battery surface temperature measurements and/or estimation of core temperatures. However, aging-induced changes in the battery model and limited training data remain major challenges for model-based and machine-learning based battery state estimation and diagnostics. To address these issues, we propose a Kolomogorov-Arnold network (KAN) in conjunction with a Koopman-based detection algorithm that leverages the unique advantages of both methods. Firstly, the lightweight KAN provides a model-free estimation of the core temperature to ensure rapid detection of battery thermal anomalies. Secondly, the Koopman operator is learned in real time using the estimated core temperature from KAN and the measured surface temperature of the battery to provide a prediction for diagnostic residual generation. This online learning approach overcomes the challenges of model changes, while the KAN-Koopman integrated structure reduces the dependence on large datasets. Furthermore, we derive analytical conditions that provide diagnostic guarantees on our KAN-Koopman detection scheme. Our simulation results illustrate a significant reduction in detection time with the proposed algorithm compared to the baseline Koopman-only algorithm.

1 Introduction

Thermal safety of batteries remains a major concern with increasing deployment of batteries in diverse applications ranging from consumer electronics to electric vehicles [1]. Thermal anomalies in the battery can lead to overheating, accelerated degradation, or even uncontrollable thermal runaway, resulting in fire, venting, or electrolyte leakage [2, 3]. Therefore, early detection of thermal anomalies is crucial to prevent catastrophic failures [4]. Consequently, [4] proposed a 1D distributed parameter model-integrated observer for thermal fault detection and estimation in a cylindrical battery. Similarly, [5] proposed a two-state thermal model-based algorithm to identify thermal faults. Furthermore, [6] optimized sensor location to improve thermal fault detectability and isolability in a pouch cell and proposed a bank of diagnostic filters for each sensor zone. [2] adopted a Chebyshev-Galerkin-based model to construct the spatial basis function with time coefficients to detect and localize thermal faults. [1] utilizes the temperature-dependent deviation of cell-impedance for early thermal fault detection. Moreover, [3], proposed a thermal fault detector that uses battery internal resistance estimation and surface temperature measurements. A set-based fault detection using constrained zonotopes was proposed in [7]. However, the effectiveness of model-based methods heavily depends on parameter reliability, and such methods exhibit a high computational complexity [8].

To overcome this limitation, [9] proposed a long short-term memory (LSTM)-based neural network (NN) model that utilizes surface temperature for thermal fault detection. Moreover, [10] adopted the discrete Fréchet distance and local outlier factor to detect and identify faulty battery cells. Additionally, physics-informed NN model [11] and Principal Component Analysis with mean-based residual generation [12] have been adopted to detect battery thermal

anomalies. Nevertheless, the data-driven approaches require a large amount of data and frequently become inefficient for unforeseen anomalies [6]. Additionally, both model-based and data-driven methods exhibit poor adaptability with varied operating conditions and battery aging [13].

Authors proposed a model-free Koopman operator-based detection of internal short circuit- [14] and corrupted charging- [13] induced thermal anomalies in the battery. In addition, the proposed algorithms adopt an online-learning framework that utilizes the limited available data and exhibits an improved adaptability with changes in battery dynamics. However, the methods rely on battery voltage and surface temperature measurements, which can lead to delayed detection of thermal anomalies [15]. Furthermore, while incorporating core temperature information can significantly aid in early detection of thermal anomalies, online core temperature measurement, even with embedded micro-sensors, remains impractical during real-world applications due to its intrusive nature and manufacturing limitations [8]. To address these research gaps, main contributions of this paper are as follows:

1. We propose a model-free Kolmogorov-Arnold network (KAN) integrated Koopman-based diagnostic algorithm for the detection of battery thermal anomalies.
2. We incorporate KAN-based core temperature estimation to ensure faster detection of thermal anomalies.
3. We derive analytical conditions to obtain diagnostic guarantees for our proposed method.

The rest of the paper is organized as follows. Section 2 presents a brief overview of KAN network and Koopman operator and Section 3 describes our problem framework. In Section 4, we introduce our proposed KAN-Koopman diagnostic algorithm. The simulation results are presented in Section 5. Finally, Section 6 concludes the paper.

2 Preliminaries

2.1 Kolmogorov-Arnold network

Kolmogorov-Arnold network (KAN) has emerged as a promising deep learning model that offers enhanced robustness and precision with a lightweight structure [16]. A NN utilizes learnable edge weights and fixed nonlinear activation functions on the output nodes for effective learning. In contrast, KAN employs learnable nonlinear activation functions on the edges that are added at output nodes for improved nonlinearity representation. Let us consider a D -deep KAN network such that the d^{th} KAN layer $\forall d \in \{1, \dots, D\}$ has ω_d input nodes (a width of ω_d) and ω_{d+1} output nodes, and these output nodes become the input nodes for the next layer $d + 1$. The a^{th} input node and the b^{th} output node in layer d , respectively, represent single variables $\alpha_{d,a}$ and $\alpha_{d+1,b}$. Then, $\forall a \in \{1, \dots, \omega_d\}$ and $\forall b \in \{1, \dots, \omega_{d+1}\}$, $\alpha_{d,a}$ pass through the activation functions $\varphi_{d,b,a}$ and then they are added to get the output variables $\alpha_{d+1,b}$, i.e. $\alpha_{d+1,b} = \sum_{a=1}^{\omega_d} \varphi_{d,b,a}(\alpha_{d,a})$. In a compact matrix form, we obtain:

$$\alpha_{d+1} = \phi_d \alpha_d, \quad \text{where } \alpha_{(\cdot)} = [\alpha_{(\cdot),1} \dots \alpha_{(\cdot),\omega_{(\cdot)}}]^T, \quad (1)$$

$$\phi_d := \begin{pmatrix} \varphi_{d,1,1} & \dots & \varphi_{d,1,\omega_d} \\ \vdots & \ddots & \vdots \\ \varphi_{d,\omega_{d+1},1} & \dots & \varphi_{d,\omega_{d+1},\omega_d} \end{pmatrix}. \quad (2)$$

ϕ_d is the activation function matrix at layer d . Following [16], to represent the activation functions in ϕ_d , we consider a weighted sum of a silu basis function and a spline function that is learn as a linear combination of κ -order B-splines over $G + 1$ grid points (G intervals). During approximating a function with such a KAN network, we can find a bound for error using the approximation theory (Theorem 2.1) presented in [16]. We briefly restate the theorem below.

Theorem 1 (Approximation Theory [16]). *Let us consider a bounded multi-variate function $f(\alpha)$ for $\alpha = (\alpha_1, \dots, \alpha_n)$ that can be expressed with finite additive compositions of $\kappa + 1$ times differentiable univariate functions $\varphi_{d,b,a}$ such that $f(\alpha) = (\phi_D \circ \phi_{D-1} \circ \dots \circ \phi_1)\alpha$, where the function matrix $\phi_d, \forall d \in \{1, \dots, D\}$ is defined in (2). Let us also consider a D -layer KAN network to approximate this function $f(\alpha)$. Then, there exists κ^{th} order B-spline functions $\varphi_{d,b,a}^G$ learned over a finite grid size G such that the bound on approximation error for the KAN network is:*

$$|f - (\phi_D^G \circ \phi_{D-1}^G \circ \dots \circ \phi_1^G)|_\infty \leq \mathcal{D}G^{-\kappa+1}, \quad (3)$$

where, the constant \mathcal{D} depends on the function and its representation, and $|\cdot|_\infty$ denotes the l_∞ norm.

We will use the findings from this theorem later for our proposed algorithm.

2.2 Koopman operator

Koopman operator (KO) is a powerful tool for model-free analysis of dynamical systems with uncertainty, nonlinearity, and complexity using computationally efficient algorithms and limited data [17]. Let us define the nonlinear dynamics of the system as $x_{k+1} = g(x_k, u_k)$ with measurements $y_k = h(x_k)$. Here $x \in \mathbb{R}^i$, $u \in \mathbb{R}^j$, and $y \in \mathbb{R}^l$ are, respectively, state vector, control input, and measured output. $h : \mathbf{X} \rightarrow \mathbb{R}^l$ denotes the nonlinear output function, and the system dynamics $g : \mathbb{R}^i \times \mathbb{R}^j \rightarrow \mathbb{R}^i$ is a continuously differentiable nonlinear function. To define KO to approximate this system, let us consider an infinite-dimensional Hilbert space of observable functions \mathcal{F} . Then, the set of KO on this space, $\mathcal{K} : \mathcal{F} \rightarrow \mathcal{F}$ is defined using the complex-valued Koopman eigenfunctions (KEF), $\theta \in \mathcal{F}$ such that $\theta : \mathbb{R}^i \rightarrow \mathbb{C}$, and the corresponding Koopman eigenvalues (KEV), $\lambda \in \mathbb{C}$, as [17]:

$$[\mathcal{K}\theta](x_k, u_k) = \theta(g(x_k, u_k)) = \lambda\theta(x_k, u_k); \quad (4)$$

We assume that the space \mathcal{F} is spanned by infinitely many KEFs as $\mathcal{F} = \text{span}\{\theta_p\}_{p=1}^{\infty}$ and the output function $h(x_k)$ also lies on \mathcal{F} . Then $h(x)$ can be expanded in terms of KEFs as $h(x_k) = \sum_{p=1}^{\infty} \theta_p(x_k, u_k) v_p^h$ [18]. Here the Koopman Modes (KM) $v_p^h \in \mathbb{C}^l$ are the projection coefficients of $h(x)$ onto the space \mathcal{F} . Next, we utilize the delay embedding to obtain the finite approximation of the linear model as $z_{k+1} = Az_k + Bu_k$; $y_k = Cz_k$ [17]. Here, z_k , A , B , and C contain, respectively, the KEFs θ_i s, KEVs λ_i s, and KMs v_i^h s. We deploy delay embedding over a moving learning window of W_l observations to approximate the Koopman model, and generate predictions for the next W_p observations, such that the generated predictions for y_k and the evolved KEFs z_k over W_p remain bounded. The windows slide ahead with W_p amount after each cycle of prediction. In particular, we rearrange the available data during the learning window to obtain a Hankel matrix X_b using the first $W_l - 1$ observations, a shifted matrix X_s using the last $W_l - 1$ observations, and an input matrix U_b (detailed formulation of these matrices can be found in [13]). Then, the Koopman model can be approximated solving the optimization problems posed as:

$$\min_{\Lambda} \|X_s - \Lambda \Upsilon\|, \quad \min_C \|Y_b - CX_b\|. \quad (5)$$

Here, $\Upsilon^T = [X_b \ U_b]$, $\Lambda = [A \ B]$. With these preliminaries on KAN and KO, next, we discuss our problem framework.

3 Thermal Anomalies in Battery

Thermal anomalies in a battery cause unanticipated heat generation, leading to overheating or even catastrophic thermal runaway failure. In our framework, we consider two classes of anomalies for such abnormal thermal behavior.

(I.) Physical faults: Several factors such as short circuits, cell-reactions, electrolyte leakage, and manufacturing malfunctions can result in thermal anomalies in the battery [6].

(II.) Compromised charging: An adversary can corrupt the charging command from cloud-BMS, leading to excessive and unwanted ohmic heat generation in the battery [13].

Mathematically, we model the battery thermal dynamics under such anomalies as follows.

$$T_{1_{k+1}} = T_{1_k} + \Delta t \left[-\frac{T_{1_k} - T_{2_k}}{R_1 C_1} + \frac{\dot{Q}_k}{C_1} + \frac{\bar{\delta}_{1_k}}{C_1} \right], \quad (6)$$

$$T_{2_{k+1}} = T_{2_k} + \Delta t \left[-\frac{T_{2_k} - T_{1_k}}{R_1 C_2} - \frac{T_{2_k} - T_{\infty_k}}{R_2 C_2} \right], \quad (7)$$

$$T_{\infty_{k+1}} = T_{\infty_k} + \Delta t \left[-\frac{T_{\infty_k} - T_{2_k}}{R_2 C_{\infty}} - \frac{\dot{Q}_{c_k}}{C_{\infty}} \right], \quad (8)$$

$$\dot{Q}_k = (I_k + \delta_{2_k})(V_{O_k}(\mathbf{s}_k) - V_{t_k} - T_{1_k}\gamma). \quad (9)$$

Here, T_1, T_2, T_{∞} are the temperatures and C_1, C_2, C_{∞} are the heat capacities of the battery core, surface, and coolant materials, respectively. R_1 and R_2 denote the thermal resistances, respectively, between the core & surface, and the surface & coolant. \dot{Q} is the internal heat generation, \dot{Q}_c is the coolant power, and γ is the entropic heat coefficient. Moreover, I is the charging current, s is the state-of-charge (SOC), V_O is the open-circuit voltage, and V_t is the terminal voltage of the battery. $\bar{\delta}_1$ and δ_2 denote thermal anomalies, where δ_2 can be induced from either a physical fault or a cyberattack, and only a physical fault can induce $\bar{\delta}_1$. Δt is the sampling time. Battery electrical dynamics is defined as

$$\mathbf{s}_{k+1} = \mathbf{s}_k - \frac{\Delta t \tilde{I}_k}{C_b}, \quad V_{t_k} = V_{O_k}(\mathbf{s}_k) - \tilde{I}_k R_b. \quad (10)$$

Here, $\tilde{I}_k = I_k + \delta_{2k}$ is corrupted charging actuation, C_b is the discharge capacity, and R_b is the internal resistance of the battery. Furthermore, substituting V_t in (9), we get $\dot{Q}_k = \tilde{I}_k^2 R_b - \tilde{I}_k T_{1k} \gamma$. We consider that temperature measurements of the surface T_2 and ambient T_∞ , along with the nominal current input I , and coolant input \dot{Q}_c are available to us.

4 KAN-Koopman Diagnostic Algorithm

The KAN-Koopman-based detection algorithm has three main steps: (i) Estimation of core temperature using an offline-trained KAN network. (ii) Predictions of core and surface temperature using an online-learned Koopman model. (iii) Generation of diagnostic residual as Koopman prediction errors to detect thermal anomalies. The algorithm addresses the challenges in battery thermal diagnostics as follows.

(I) Model-free approach: Our proposed algorithm adopts a data-driven approach to detect thermal anomalies using only the available data ($T_2, T_\infty, I, \dot{Q}_c$), and without relying on the prior model knowledge of battery thermal dynamics.

(II) Enhanced thermal information with KAN-based T_1 estimation: The algorithm trains a KAN network to effectively learn intrinsic thermal patterns offline, where T_1 measurements can be accessed using a lab experimental set-up or high-fidelity simulations. The trained KAN model is then deployed to generate T_1 estimations online.

(III) Adaptive residual generation with Koopman model: The offline-trained KAN model fails to account for unforeseen changes in operating conditions. Koopman module, on the other hand, learns the variability in battery dynamics from T_2 measurements, thereby overcoming the poor adaptability of the KAN network.

Thus, the proposed KAN-Koopman diagnostic algorithm leverages the unique advantages of each method to ensure rapid detection of thermal anomalies with improved adaptability to changes in battery dynamics.

4.1 KAN-based estimation

To estimate the core temperature T_1 , we adopt the KAN-Therm model proposed in our previous work [19]. The proposed KAN model uses four input features as:

$$\mathbb{T}_{1k} = \text{KAN}(\boldsymbol{\alpha}_k), \quad \boldsymbol{\alpha}_k = [T_{2k} \quad T_{\infty k} \quad I_k \quad \dot{Q}_{ck}]^T. \quad (11)$$

Here, \mathbb{T}_{1k} is the estimation of T_1 at k^{th} instant, and the estimation error $e_k = \mathbb{T}_{1k} - T_{1k}$. From (6), we can rewrite the core temperature dynamics as $T_{1k} = F(\boldsymbol{\alpha}_k)$, where $F(\boldsymbol{\alpha}_k)$ is the solution of (6). Since the underlying battery dynamics is Lipschitz continuous, we can find a Lipschitz constant $L_F \in \mathbb{R}^+$, such that F is Lipschitz continuous in $\boldsymbol{\alpha}_k$:

$$\|F(\boldsymbol{\alpha}_k) - F(\boldsymbol{\alpha}_k + \Delta\boldsymbol{\alpha}_k)\| \leq L_F \|\Delta\boldsymbol{\alpha}_k\|, \quad \forall k. \quad (12)$$

Under thermal anomalies, the true $T_{1k} = F(\boldsymbol{\alpha}_k + \delta_k) + \delta_{1k}$, whereas the KAN network estimates \mathbb{T}_{1k} using $\boldsymbol{\alpha}_k$. Here, $\delta_k := [0 \quad 0 \quad \delta_{2k} \quad 0]^T \neq 0$ and $\delta_{1k} \neq 0$ is a function of thermal fault $\bar{\delta}_{1k}$. Thus, we can write e_k in terms of δ_k and δ_{1k} as

$$\|e_k(\delta_k, \delta_{1k})\| = \|\text{KAN}(\boldsymbol{\alpha}_k) - F(\boldsymbol{\alpha}_k + \delta_k) - \delta_{1k}\|. \quad (13)$$

Under nominal battery operation $\|\delta_k\| = 0$ and $\delta_{1k} = 0$, the estimation error $e_k(\mathbf{0}, 0) = \mathbb{T}_{1k} - T_{1k} = \text{KAN}(\boldsymbol{\alpha}_k) - F(\boldsymbol{\alpha}_k)$. Hence, using the KAN approximation Theorem 1,

$$|e_k(\mathbf{0}, 0)|_\infty \leq \mathcal{D}G^{-\kappa+1}, \quad \forall k. \quad (14)$$

Lemma 1 (Lipschitz continuity of error with anomalies). *Consider the bounded multi-variate function $F(\boldsymbol{\alpha}_k)$ that is Lipschitz continuous in $\boldsymbol{\alpha}_k$ (12) and can be expressed with KAN ($\boldsymbol{\alpha}_k$) network (11). Under nominal battery operation ($\|\delta_k\|, \delta_{1k}=0$), (14) provides the approximation error bound for KAN ($\boldsymbol{\alpha}_k$). Then, under anomalous input $\|\delta_k\|, \delta_{1k} \neq 0$, the KAN approximation error $e_k(\delta_k, \delta_{1k})$ is Lipschitz continuous in δ_k, δ_{1k} , with Lipschitz constant $L_e > 0$, i.e.,*

$$\|e_k(\delta_k, \delta_{1k}) - e_k(0, 0)\| \leq L_e \left[\|\delta_{1k}\| + \|\delta_k\| \right], \quad \forall k. \quad (15)$$

Proof. Under thermal anomaly, consider (13) to add and subtract $F(\boldsymbol{\alpha}_k)$ on the right-hand side (RHS) to obtain

$$\|e_k\| = \|\text{KAN}(\boldsymbol{\alpha}_k) - F(\boldsymbol{\alpha}_k) - \delta_{1k} + F(\boldsymbol{\alpha}_k) - F(\boldsymbol{\alpha}_k + \delta_k)\|. \quad (16)$$

Then, using the triangular inequality, (16) becomes

$$\|e_k\| \leq \|\text{KAN}(\boldsymbol{\alpha}_k) - F(\boldsymbol{\alpha}_k)\| + \|\delta_{1k}\| + \|F(\boldsymbol{\alpha}_k) - F(\boldsymbol{\alpha}_k + \delta_k)\|. \quad (17)$$

Next, using Lipschitz continuity of F and (14) yields

$$\|e_k\| \leq \|e_k(\mathbf{0}, 0)\| + \|\delta_{1_k}\| + L_F \|\delta_k\|. \quad (18)$$

Furthermore, subtracting $\|e_k(\mathbf{0}, 0)\|$ on each side of the inequality and choosing $L_e := \max(1, L_F)$ we prove (15). \blacksquare

Remark 1. Lemma 1 implies that the error $e_k(\delta_k, \delta_{1_k})$ in KAN estimate is Lipschitz continuous in δ_k, δ_{1_k} , and thus, also absolutely continuous in δ_k, δ_{1_k} . This regularity of $e_k(\delta_k, \delta_{1_k})$ in δ_k, δ_{1_k} implies that the KAN-based core temperature estimation \mathbb{T}_1 will vary regularly with thermal anomalies. Thus, the KAN estimate can be utilized reliably as a measurement proxy even under anomalous thermal conditions for the following Koopman module. This result is strong as it guarantees the KAN network behavior under anomalous inputs that are beyond the nominal training set.

4.2 Koopman-based prediction

We use KO to generate the core and surface temperature predictions $\hat{\mathbb{T}}_1$ and $\hat{\mathbb{T}}_2$ using KAN estimate and available data as $\mathbf{y}_k = [\mathbb{T}_{1_k} \quad \mathbb{T}_{2_k}]^T$ and $u_k = [I_k \quad T_{\infty k}]^T$. Then, adopting the delay-embedding technique discussed in Section 2.2 and using (5), we can first learn the Koopman linear model over a sliding learning window of length W_l and then generate the predictions $\hat{\mathbf{y}}$ and the detection residual \mathbf{r}_k over the following prediction window of length W_p as:

$$\mathbf{z}_{k+1} = \mathbf{A}\mathbf{z}_k + \mathbf{B}u_k; \quad \hat{\mathbf{y}}_k = \mathbf{C}\mathbf{z}_k, \quad \mathbf{r}_k = \|\mathbf{y}_k - \hat{\mathbf{y}}_k\|. \quad (19)$$

4.3 Diagnostic guarantees

To obtain the diagnostic guarantees for the residual \mathbf{r}_k , let us first consider a hypothetical Koopman model that can access the true core temperature measurement T_1 such that $y_k = [T_{1_k} \quad T_{2_k}]^T$ and the prediction \hat{y} , residual r_k are defined as

$$z_{k+1} = Az_k + Bu_k, \quad \hat{y}_k = Cz_k, \quad r_k = \|y_k - \hat{y}_k\|. \quad (20)$$

Our previous work in [20] shows that in the presence of anomalies, for a Koopman model that learns from true system measurement, r_k will cross the threshold reliably to detect the anomalous input. Hence, we assume that for the hypothetical model described above, there exist a constant $M_1 \in \mathbb{R}^+$ and practical relaxation constant $\epsilon_M > 0$, such that

$$\|r_k\| \geq M_1 [\|\delta_k\| + \|\delta_{1_k}\|] - \epsilon_M, \quad \forall k. \quad (21)$$

This sensitivity constant $M_1 \geq 1$ is a design parameter, and a higher value of M_1 ensures the detection of smaller-valued δ_k, δ_{1_k} . Furthermore, under no thermal anomalies, the hypothetical residual must remain below the threshold to avoid false detection, i.e. for $\|\delta_k\| = \delta_{1_k} = 0$, $\|r_k\| \leq \epsilon_M$. Next, we will present the two main theorems for our KAN-Koopman framework using these conditions on r_k .

Theorem 2 (Upper bound on residual under no anomaly). *Consider the proposed KAN-Koopman model (19) learned using the KAN estimate \mathbb{T}_1 and the hypothetical Koopman model (20) using true measurement T_1 . Then, during nominal battery operation ($\|\delta_k\|, \delta_{1_k} = 0$), the diagnostic residual \mathbf{r}_k is bounded for $\beta_1, \beta_2 \in \mathbb{R}^+$ and $\varsigma_k = \beta_1 \|C\| + \beta_2 \|\mathbf{z}_k\|$ as:*

$$\mathbf{r}_k \leq r_k + (1 + \varsigma_k) \sqrt{2} \mathcal{D} G^{-\kappa+1}, \quad \forall k. \quad (22)$$

Proof. Let us expand the residual \mathbf{r}_k as:

$$\mathbf{r}_k = \|\mathbf{y}_k - \mathbf{C}\mathbf{z}_k\| = \|(\mathbf{y}_k - y_k) + (y_k - Cz_k) + (Cz_k - \mathbf{C}\mathbf{z}_k) + (\mathbf{C}\mathbf{z}_k - \mathbf{C}\mathbf{z}_k)\|. \quad (23)$$

Defining $\Delta C := C - \mathbf{C}$, we use the triangular inequality on RHS of (23) and substitute (20) to obtain

$$\mathbf{r}_k \leq r_k + \|\mathbf{y}_k - y_k\| + \|C\| \|z_k - \mathbf{z}_k\| + \|\Delta C \mathbf{z}_k\|. \quad (24)$$

Let us denote $\xi_k = \mathbf{y}_k - y_k$. Then, $\xi_k = [e_k \quad 0]^T$ since the surface temperature T_2 is known. Hence, we obtain

$$\|\xi_k\| = \|\mathbf{y}_k - y_k\| = \|e_k\|. \quad (25)$$

Next, the KMs can be found analytically using (5) as

$$\mathbf{C} = \mathbf{Y}_b \mathbf{X}_b^T (\mathbf{X}_b \mathbf{X}_b^T)^{-1}, \quad C = Y_b X_b^T (X_b X_b^T)^{-1}. \quad (26)$$

Here, \mathbf{Y}_b and Y_b are the delay-embedded measurements for the proposed and hypothetical Koopman models, respectively. Additionally, \mathbf{z}_k and z_k are the single columns in the Hankel matrices \mathbf{X}_b and X_b , respectively. These matrices \mathbf{X}_b and X_b contain, respectively, a time-delayed sequence of \mathbf{y}, u data and y, u data from previous $k - W_l$ observations. Thus, $\Delta z_k = \mathbf{z}_k - z_k$, $\Xi = Y_b - \mathbf{Y}_b$, and $\zeta = X_b - \mathbf{X}_b$ contain 0 and ξ_j as their entries for $j \in \mathcal{J} := \{k, \dots, k - W_l\}$. Let us now define a constant $\beta_1 > 0$ such that $\beta_1 \|\xi_k\| \geq W_l \max_{j \in \mathcal{J}} (\|\xi_j\|)$ and then, we can obtain the bounds as

$$\|\Delta z_k\| \leq \beta_1 \|\xi_k\|, \quad \|\Xi\| \leq \beta_1 \|\xi_k\|, \quad \|\zeta\| \leq \beta_1 \|\xi_k\|. \quad (27)$$

Now, substituting $\mathbf{Y}_b = Y_b - \Xi$ and $\mathbf{X}_b = X_b - \zeta$ in the first equation of (26), we obtain

$$\mathbf{C} = [Y_b - \Xi][X_b - \zeta]^T \left([X_b - \zeta][X_b - \zeta]^T \right)^{-1} \quad (28)$$

$$= [Y_b - \Xi][X_b - \zeta]^T \left(X_b X_b^T - \eta \right)^{-1}, \quad (29)$$

where $\eta = X_b \zeta^T + \zeta X_b^T - \zeta \zeta^T$. Now, taking l_2 norm and using the triangular inequality, we can write $\|\eta\| \leq 2\|X_b\|\|\zeta\| + \|\zeta\|^2$. Next, using the boundness of the Hankel matrix X_b and ζ from (27), we can find a constant $\beta_3 \in \mathbb{R}^+$ such that we get $\|\eta\| \leq \beta_3 \|\xi_k\|$. Next, multiplying $(X_b X_b^T)^{-1} X_b X_b^T$ with $(X_b X_b^T - \eta)^{-1}$ from left and merging $X_b X_b^T$, we get

$$\begin{aligned} \mathbf{C} &= [Y_b - \Xi][X_b - \zeta]^T (X_b X_b^T)^{-1} (I - N)^{-1} \\ &= C(I - N)^{-1} - \mu, \quad \text{where } N = (X_b X_b^T)^{-1} \eta, \end{aligned} \quad (30)$$

$$\mu = [Y_b \zeta^T + \Xi X_b^T - \Xi \zeta^T] (X_b X_b^T)^{-1} (I - N)^{-1}. \quad (31)$$

Now, taking l_2 norm on μ and considering the boundness of X_b and Y_b , we can use (27) to obtain a $\beta_4 \in \mathbb{R}^+$ such that $\|\mu\| \leq \beta_4 \|\xi_k\|$. Next, subtracting C on both sides of (30), using definition of N (30) after simplification, we can obtain

$$\Delta C = C (X_b X_b^T)^{-1} \eta \left(I - (X_b X_b^T)^{-1} \eta \right)^{-1} - \mu. \quad (32)$$

Notice that ΔC contains η , μ , and bounded terms. Thus, using the bounds on η , μ , we can obtain $\beta_2 \in \mathbb{R}^+$ such that

$$\|\Delta C\| \leq \beta_2 \|\xi_k\|. \quad (33)$$

Finally, using (25), (27), and (33), we can rewrite (24) as:

$$\mathbf{r}_k \leq r_k + (1 + \varsigma_k) \|e_k\|, \quad (34)$$

where $\varsigma_k = \beta_1 \|C\| + \beta_2 \|\mathbf{z}_k\|$. Furthermore, in the absence of thermal anomalies, i.e., $\|\delta_k\|, \delta_{1_k} = 0$, (34) becomes

$$\mathbf{r}_k \leq r_k + (1 + \varsigma_k) \|e_k(\mathbf{0}, 0)\|. \quad (35)$$

Additionally, from (14), and using definitions of l_2 and l_∞ norm, we can get $\|e_k(\mathbf{0}, 0)\| \leq \sqrt{2} |e_k(\mathbf{0}, 0)|_\infty \leq \sqrt{2} \mathcal{D} G^{-\kappa+1}$. Finally, substituting this bound for $\|e_k(\mathbf{0}, 0)\|$ in (35), we can obtain (22). This completes the proof. ■

Theorem 2 shows that during nominal battery operation ($\|\delta_k\|, \delta_{1_k} = 0$), the residual \mathbf{r}_k remains close to zero since r_k is bounded by ϵ_M and the KAN approximation can be made arbitrarily small depending on the network structure i.e. with higher grid G and activation function order κ .

Theorem 3 (Reliable detection of thermal anomalies). *Consider the proposed KAN-Koopman model (19) learned using the KAN estimate \mathbb{T}_1 and the hypothetical Koopman model (20) learned using true measurement T_1 . Then, for thermal anomalies δ_k and δ_{1_k} satisfying (37), the bound for residual $\mathbf{r}_k, \forall k$ can be found for positive constants $M_1, M_2 \in \mathbb{R}^+$ as:*

$$\mathbf{r}_k \geq [M_1 - M_2] \left[\|\delta_{1_k}\| + \|\delta_k\| \right] - \epsilon_M - (1 + \varsigma_k) \|e_k(\mathbf{0}, 0)\|. \quad (36)$$

$$\|\delta_{1_k}\| + \|\delta_k\| \geq \epsilon_M + \varsigma_k \sqrt{2} \mathcal{D} G^{-\kappa+1}. \quad (37)$$

Proof. For thermal anomalies δ_k and δ_{1_k} satisfying (37), using the inverse triangular inequality on the RHS of (23), and using the bounds from (27) and (33), (23) becomes

$$\mathbf{r}_k \geq r_k - (1 + \varsigma_k) \|e_k\|. \quad (38)$$

Next, from Lemma 1, we can obtain $\|e_k\| \geq -\|e_k(\mathbf{0}, 0)\| - L_e \left[\|\delta_{1_k}\| + \|\delta_k\| \right]$. Then, using this bound to substitute $\|e_k\|$ and using (21) to substitute r_k in (38), we obtain

$$r_k \geq [M_1 - L_e(1 + \varsigma_k)] \left[\|\delta_{1_k}\| + \|\delta_k\| \right] - \epsilon_M - (1 + \varsigma_k) \|e_k(\mathbf{0}, 0)\|. \quad (39)$$

Now, let $M_2 = L_e(1 + \varsigma_k)$. Then we can rewrite (39) as (36), which completes the proof. \blacksquare

Theorem 3 implies that if the sensitivity parameter M_1 is chosen as $M_1 \geq M_2$, the diagnostic residual r_k can ensure the reliable detection of thermal anomalies δ_{1_k} and δ_k that satisfy (37), and satisfying (37) indicates thermal anomalies with values greater than the bound of the KAN approximation error $e_k(\mathbf{0}, 0)$ and the practical relaxation factor ϵ_M . Thus, if $e_k(\mathbf{0}, 0)$ is kept small enough with the appropriate network structure (grid G and spline order κ), the proposed KAN-Koopman algorithm can reliably detect low-magnitude thermal anomalies in battery.

5 Simulation Results

We consider a 2.3Ah cylindrical $LiFePO_4 - LiC_6$ battery cell for our case studies and adopt the model parameters from [21]. We consider a sampling frequency of 100Hz and a zero-mean Gaussian measurement noise of $\pm 0.05^\circ$ for the T_1, T_2 , and T_∞ measurements. Next, we provide details of the KAN-Koopman model and present two thermal anomaly scenarios to evaluate our proposed algorithm's performance.

5.1 Details of KAN-Koopman implementation

KAN architecture: We consider a two-layered KAN network with a network configuration of $\llbracket 4, 3, 1 \rrbracket$: input layer with width 4 (four features $T_2, T_\infty, I, \dot{Q}_c$), followed by a KAN layer of width 3, and the final KAN layer of width 1 (single output T_1). This architecture contains a total of 15 learnable activation functions, 12 in the 1st and 3 in the 2nd KAN layer. Furthermore, we consider the grid $G = 5$ and spline order $\kappa = 3$ to approximate the learnable functions.

Koopman parameters: We consider a learning window of length 3000 data-points (30s) with delay-embedding length of 2100 to generate predictions for the next 500 observations (5s). Furthermore, we choose a threshold of 0.03 based on the nominal fluctuations in residual r under $\|\delta_k\|, \delta_{1_k} = 0$. We have used the average of generated residuals over a moving window of 3000 to reduce the setting and resetting of the attack detection flag during threshold crossings.

5.2 Case study I: Incipient thermal fault

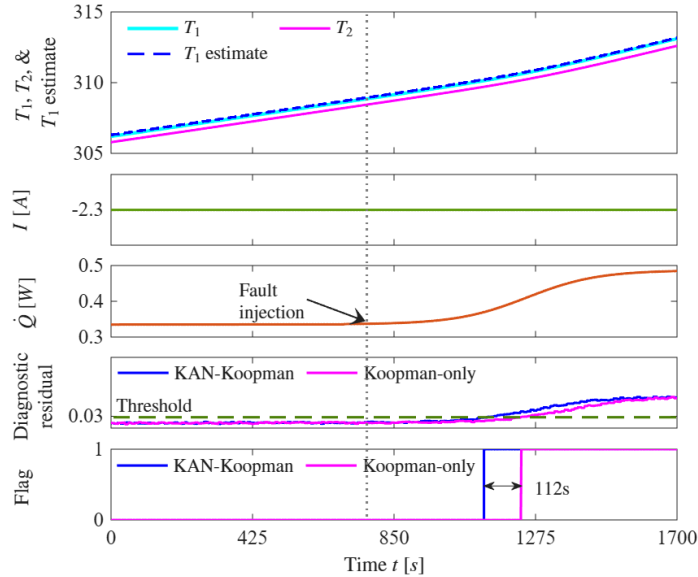


Figure 1: Under an incipient thermal fault, top plot shows T_1, T_2 , and T_1 ; second plot shows I ; third plot shows \dot{Q} ; fourth and fifth plots, respectively, shows the diagnostic residuals and the thermal anomaly flag generated by proposed and the baseline Koopman algorithm.

In this scenario, we consider that the battery is charging at $1C$ rate and an incipient thermal fault δ_1 is injected from 800s. Due to the slow-progressing nature of the injected fault, T_1 and T_2 do not exhibit any abrupt growth in temperatures, as shown in the top plot of Fig 1. The second plot of Fig 1 shows the charging current, and the third plot illustrates the increased heat generation in the battery after the incipient fault injection. Under such thermal anomaly, our diagnostic residual r crosses the threshold at 1112s as shown in the fourth plot of Fig 1, resulting in a reliable detection of the thermal anomaly after 362s of the fault occurrence (shown by setting of the anomaly flag in the last plot). We also compare this performance with a baseline Koopman-only algorithm that solely relies on T_2 measurement for diagnosis. The last plot of Fig 1 shows that the baseline method takes 112s longer than the proposed method to generate the anomaly flag. Thus, the proposed method exhibits 24% faster detection of thermal anomalies in this scenario.

5.3 Case study II: Battery charging cyberattack

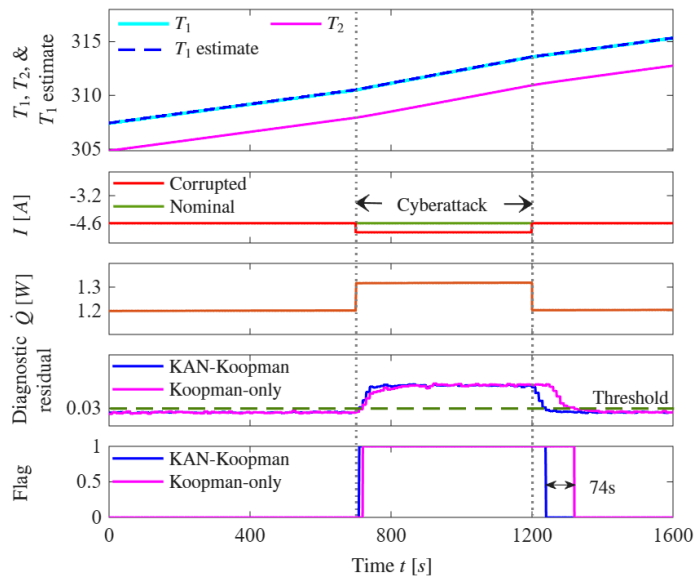


Figure 2: Under battery charging cyberattack, top plot shows T_1 , T_2 , and T_1 estimate; second plot shows nominal and corrupted I ; third plot shows \dot{Q} ; fourth and fifth plots, respectively, shows the diagnostic residuals and the thermal anomaly flag generated by proposed and the baseline Koopman algorithm.

For this case study, we consider that the battery is charging at $2C$ rate, and an adversary then injects a 10% bias attack of $-0.46A$ from 700s to 1200s. The top plot of Fig 2 shows the true core and surface temperature T_1 , T_2 , and the KAN-estimation T_1 under this compromised charging scenario. The second plot of Fig 2 shows the nominal and corrupted charging current, and the third plot captures the additional heat generation under corrupted charging. In this scenario, our diagnostic residual r crosses the threshold at 708s and thus, reliably detects the presence of thermal anomaly after 8s of attack injection (as shown in the fourth and last plot of Fig 2). The baseline Koopman algorithm detects the thermal anomaly at 720s, leading to a 12s delay in detection compared to the proposed method. Additionally, after the attack withdrawal, residuals for both methods go below the threshold and the flag is reset at 1239s and 1315s as shown the last plot of Fig 2. Thus, the KAN-Koopman method exhibits 60% faster detection and also 64% faster recovery.

6 Conclusion

In this paper, we propose a model-free KAN-Koopman diagnostic algorithm for the detection of battery thermal anomalies that can be induced from both physical faults and cyberattacks. The proposed method adopts a lightweight KAN network that estimates the core temperature, and next, a Koopman model is learned online using the KAN estimation along with the limited available data to generate predictions for the battery core and surface temperatures. This online learning approach leads to improved adaptability with changes in battery dynamics, while the KAN-Koopman integrated structure ensures rapid detection of battery thermal anomalies. The diagnostic residual is generated as the error in the Koopman predictions for the KAN-based core temperature estimation and surface temperature measurement. Furthermore, we derive analytical conditions for diagnostic guarantees on our KAN-Koopman detection scheme. We compare the performance of our model with the baseline Koopman-only model, that only utilizes surface

temperature for diagnostics. Our comparison result shows that the proposed KAN-Koopman method exhibits 24% faster detection of an incipient thermal fault induced thermal anomalies, and 60% faster detection of anomalous heat generation under corrupted charging compared to the Koopman-only model.

References

- [1] Jacob Klink, Jens Grabow, Nury Orazov, Ralf Benger, Alexander Börger, Annika Ahlberg Tidblad, Heinz Wenzl, and Hans-Peter Beck. Thermal Fault Detection By Changes In Electrical Behaviour In Lithium-ion Cells. *Journal of Power Sources*, 490:229572, 2021.
- [2] Jinhui Zhou, Wenjing Shen, Zhengwei Ma, Xiaolin Mou, Yu Zhou, Han-Xiong Li, and Liqun Chen. Chebyshev-galerkin-based Thermal Fault Detection And Localization For Pouch-type Li-ion Battery. *IEEE Transactions on Industrial Informatics*, 20(3):3436–3445, 2023.
- [3] Jingwen Wei, Guangzhong Dong, and Zonghai Chen. Lyapunov-based Thermal Fault Diagnosis Of Cylindrical Lithium-ion Batteries. *IEEE Transactions on Industrial Electronics*, 67(6):4670–4679, 2019.
- [4] Satadru Dey, Hector E Perez, and Scott J Moura. Model-based Battery Thermal Fault Diagnostics: Algorithms, Analysis, And Experiments. *IEEE Transactions on Control Systems Technology*, 27(2):576–587, 2017.
- [5] Jeongeun Son and Yuncheng Du. Model-based Stochastic Fault Detection And Diagnosis Of Lithium-ion Batteries. *Processes*, 7(1):38, 2019.
- [6] Sara Sattarzadeh, Tanushree Roy, and Satadru Dey. Thermal Fault Detection And Localization Framework For Large Format Batteries. *Journal of Power Sources*, 512:230400, 2021.
- [7] Giacomo Saccani, Diego Locatelli, Angelo Tottoli, and Davide M Raimondo. Model-based Thermal Fault Detection In Li-ion Batteries Using A Set-based Approach. *IFAC-PapersOnLine*, 55(6):329–334, 2022.
- [8] Robert R Richardson, Peter T Ireland, and David A Howey. Battery Internal Temperature Estimation By Combined Impedance And Surface Temperature Measurement. *Journal of Power Sources*, 265:254–261, 2014.
- [9] Olaoluwa Ojo, Haoxiang Lang, Youngki Kim, Xiaosong Hu, Bingxian Mu, and Xianke Lin. A Neural Network Based Method For Thermal Fault Detection In Lithium-ion Batteries. *IEEE Transactions on Industrial Electronics*, 68(5):4068–4078, 2020.
- [10] Zhenyu Sun, Zhenpo Wang, Peng Liu, Zian Qin, Yong Chen, Yang Han, Peng Wang, and Pavol Bauer. An Online Data-driven Fault Diagnosis And Thermal Runaway Early Warning For Electric Vehicle Batteries. *IEEE transactions on power electronics*, 37(10):12636–12646, 2022.
- [11] Mina Naguib, Junran Chen, Phillip Kollmeyer, and Ali Emadi. Thermal Fault Detection Of Lithium-ion Battery Packs Through An Integrated Physics And Deep Neural Network Based Model. *Communications Engineering*, 4(1):1–9, 2025.
- [12] Kiran Bhaskar, Ajith Kumar, James Bunce, Jacob Pressman, Neil Burkell, and Christopher D Rahn. Data-driven Thermal Anomaly Detection In Large Battery Packs. *Batteries*, 9(2):70, 2023.
- [13] Sanchita Ghosh and Tanushree Roy. Detection And Isolation Of Battery Charging Cyberattacks Via Koopman Operator. *Applied Energy*, 401:126695, 2025.
- [14] Sanchita Ghosh, Soumyoraj Mallick, and Tanushree Roy. Koopman Mode-based Detection Of Internal Short Circuits In Lithium-ion Battery Pack. In *2025 American Control Conference (ACC)*, pages 1777–1782. IEEE, 2025.
- [15] Dominic Karnehm, Akash Samanta, Christian Rosenmüller, Antje Neve, and Sheldon Williamson. Core Temperature Estimation Of Lithium-ion Batteries Using Long Short-term Memory (Lstm) Network And Kolmogorov-arnold Network (Kan). *IEEE Transactions on Transportation Electrification*, 2025.
- [16] Ziming Liu, Yixuan Wang, Sachin Vaidya, Fabian Ruehle, James Halverson, Marin Soljačić, Thomas Y Hou, and Max Tegmark. Kan: Kolmogorov-arnold Networks. *arXiv preprint arXiv:2404.19756*, 2024.
- [17] Marko Budišić, Ryan Mohr, and Igor Mezić. Applied Koopmanism. *Chaos: An Interdisciplinary Journal of Nonlinear Science*, 22(4), 2012.
- [18] Amit Surana and Andrzej Banaszuk. Linear Observer Synthesis For Nonlinear Systems Using Koopman Operator Framework. *IFAC-PapersOnLine*, 49(18):716–723, 2016.
- [19] Soumyoraj Mallick, Faysal Ahamed, Sanchita Ghosh, and Tanushree Roy. KAN-Therm: A Lightweight Battery Thermal Model Using Kolmogorov-Arnold Network. *arXiv preprint arXiv:2509.09145*, 2025.

- [20] Sanchita Ghosh and Tanushree Roy. Koopman Operator-based Detection-isolation Of Cyberattack: A Case Study On Electric Vehicle Charging. In *2024 American Control Conference (ACC)*, pages 2236–2241. IEEE, 2024.
- [21] Shashank Dhananjay Vyas, Tanushree Roy, and Satadru Dey. An Input-to-State Safety Approach Toward Thermal Fault-Tolerant Battery Cells. *IEEE Transactions on Control Systems Technology*, 2024.